5G Module V1.0

APPLICATION NOTE

5G Compliance Testing with DASY6

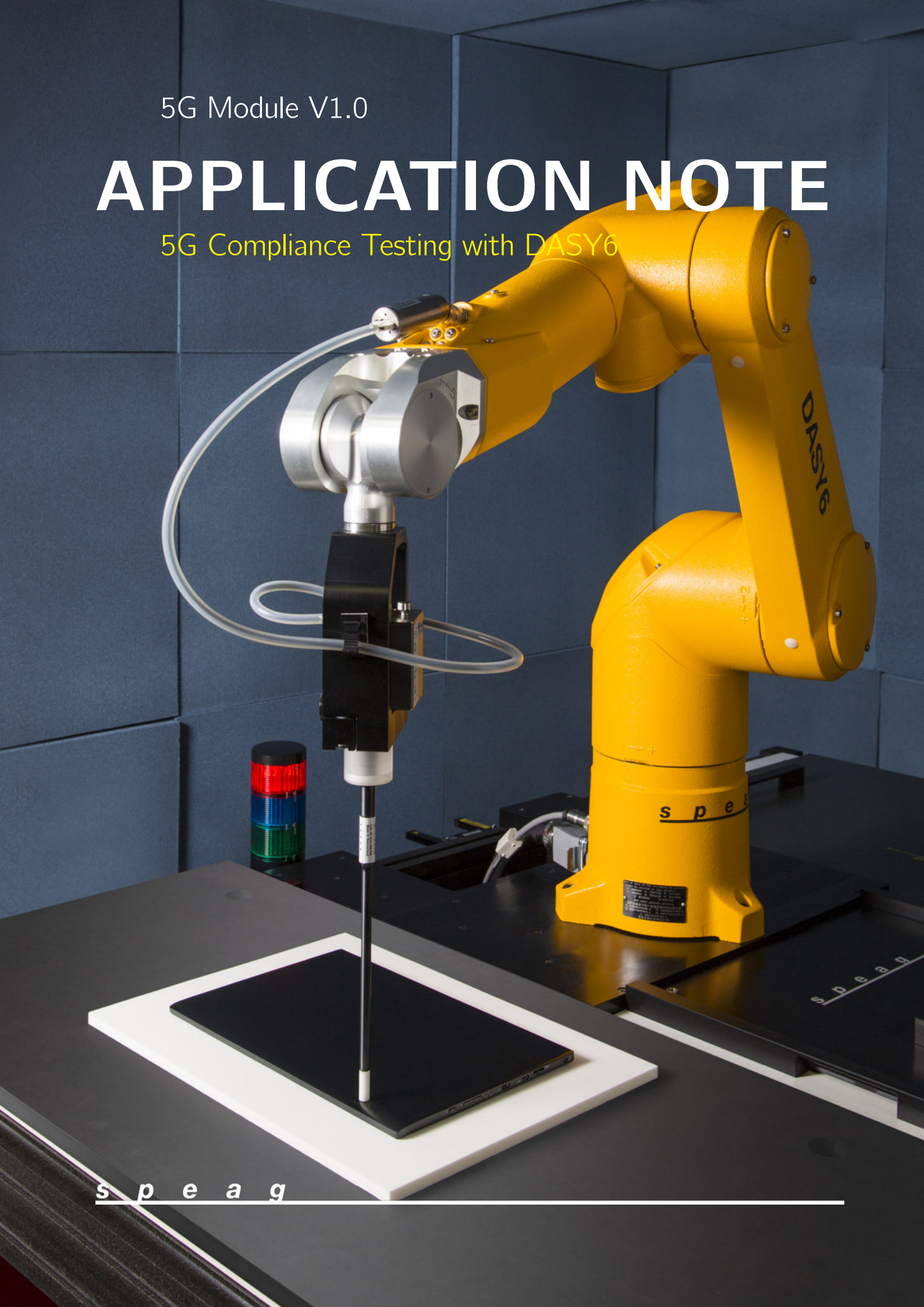

speag

5G Compliance Testing with DASY6

Release of *5G Module V1.0*

This Application Note describes the usage and performance of the 5G Module V1.0 as of August 2017. SPEAG will continue to refine and improve:

- calibration of the EUmmWV2 probe to obtain ISO17025 accreditation for the frequency range 3 – 110 GHz;
- the scanning strategy to reduce the measurement time;
- the reconstruction algorithm;
- the surface conformity assessments;
- uncertainty;
- validation up to 110 GHz;
- the user-friendliness and flexibility of the software.

1 Introduction

Fifth Generation (5G) technologies will bring communication systems that operate at millimeter-wave frequencies into mobile devices, making safety a near-field problem that will lead to new requirements on test systems for assessment of compliance with electromagnetic safety guidelines. The solution proposed in this Application Note is based on a novel non-disturbing millimeter wave near-field probe and a total-field and power-flux-density reconstruction algorithm. The applicability of the solution to test device safety has been validated for millimeter wave sources at distances as small as 2 mm.

2 EUmmWV2 Probe Description

2.1 Probe Design

The EUmmWV2 probe is based on the pseudo-vector probe design, which not only measures the field magnitude but also derives its polarization ellipse. This probe concept also has the advantage that the sensor angle errors or distortions of the field by the substrate can be largely nullified by calibration. This is particularly important as, at these very high frequencies, field distortions by the substrate are dependent on the wavelength. The design entails two small 0.8 mm dipole sensors mechanically protected by high-density foam, printed on both sides of a 0.9 mm wide and 0.12 mm thick glass substrate. The body of the probe is specifically constructed to minimize distortion by the scattered fields.
The probe consist of two sensors with different angles (γ_1 and γ_2) arranged in the same plane in the probe axis. Three or more measurements of the two sensors are taken for different probe rotational angles to derive the amplitude and polarization information. These probes are the most flexible and accurate probes currently available for measuring field amplitude.
The probe design allows measurements as close as 2 mm from the sensors to the DUT surface. The typical sensor to probe tip distance is 1.5 mm. The exact distance is calibrated.

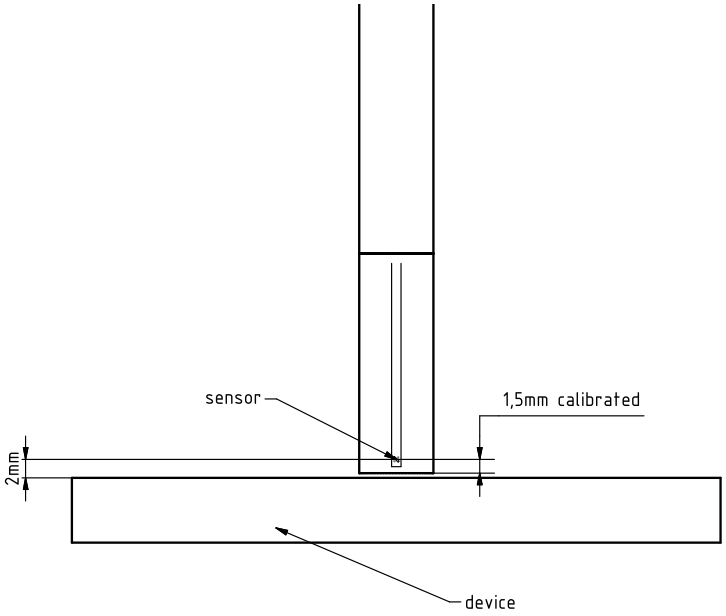

Figure 1.1: Illustration of distance sensor to DUT surface

2.2 Probe Handling

EUmmWV2 probes must be operated with specific care to avoid any damage:

- the probe must be used only in air; it is not designed to be immersed in liquids;
- the protective probe cap should be only removed for the measurements by sliding it carefully along the probe axis;
- the application of lateral force to the probe tip should be strictly avoided;
- use a dummy probe should be used to test the scanning or any robot movement before making measurements.

3 Measurements

3.1 Prerequisites

The following system configuration is required to perform 5G measurements:

- DASY6 system;
- EUmmWV2 probe;
- 5G phantom cover
- cDASY6 5G Module software with a valid license.

3.2 Hardware Configuration

First, the hardware configuration must be specified in the software. This is performed following the steps described below:

- under Application Preferences » Inventory » Phantom, import the 5G Phantom Cover;
- under Application Preferences » Inventory » TSLs (Tissue Simulating Liquids), import Air;

- under Application Preferences » Inventory » DAEs, import the DAE configuration file;
- under Application Preferences » Inventory » Probes, import the EUmmWV configuration file;
- under Hardware Setup View, select the DAE, probe, and phantom to be used during the measurements.
- insert the 5G phantom cover in one of the DASY6 system platform slot

Then, insert the 5G phantom cover in one of the slots of the DASY6 system platform. The phantom can be taught using the "Teach Phantom" entry in the context menu of the 3D view. The procedure is indentical as teaching SAR phantoms. The phantom teaching will define the inclination of the measurement plane. The last step consists of teaching the DUT. The DUT is taught by a single point. This point defines the DUT height. The measurement plane will be parallel to the phantom cover, the height is given by the DUT taught point to which the measurement distance is added. The grid will be centered on the DUT taught point.

3.3 Project Generation

Measurements can be added to the current project as described below:

- Go to Setup mode, Project Setup view.
- In Device Settings, enter the dimensions of the DUT.
- In Test Conditions, enter the desired measurement distance and click on "Add Test Condition to Project". Multiples test conditions can be added to the same measurement file. The measurement distance corresponds to the distance probe sensor to DUT.
- In Communication Systems, select the desired communication system, band and channel.

The grid steps are optimized by the software based on the test frequency. The grid extents are calculated based on the Source Radius entered by the user. These field are accessible when the measurement group line of the configuration to be measured is selected in the Project Overview window.

4 Post Processing

4.1 E-field Polarization Ellipse Computation

For the numerical description of an arbitrarily oriented ellipse in three-dimensional space, five parameters are needed: the semi-major axis (a), the semi-minor axis (b), two angles describing the orientation of the normal vector of the ellipse (ϕ, θ), and one angle describing the tilt of the semi-major axis (ψ). For the two extreme cases, i.e., circular and linear polarizations, three parameters only (a, ϕ, and θ) are sufficient for the description of the incident field.

For the reconstruction of the ellipse parameters from measured data, the problem can be reformulated as a nonlinear search problem. The semi-major and semi-minor axes of an elliptical field can be expressed as functions of the three angles (ϕ, θ, and ψ). The parameters can be uniquely determined towards minimizing the error based on least-squares for the given set of angles and the measured data. In this way, the number of free parameters is reduced from five to three, which means that at least three sensor readings are necessary to gain sufficient information for the reconstruction of the ellipse parameters. However, to suppress the noise and increase the reconstruction accuracy, it is desirable to have an overdetermined system of equations. The solution to use a probe consisting of two sensors angled by γ_1 and γ_2 toward the probe axis and to perform measurements at three angular positions of the probe, i.e., at β_1, β_2, and β_3, results in overdeterminations of two. If there is a need for more information or increased accuracy, more rotation angles can be added.

The reconstruction of the ellipse parameters can be separated into linear and non-linear parts that are best solved by the Givens algorithm combined with a downhill simplex algorithm.

To minimize the mutual coupling, sensor angles are set with a 90° shift ($\gamma_2 = \gamma_1 + 90°$), and, to simplify, the first rotation angle of the probe (β_1) can be set to 0°. Mode details can be found in [1].

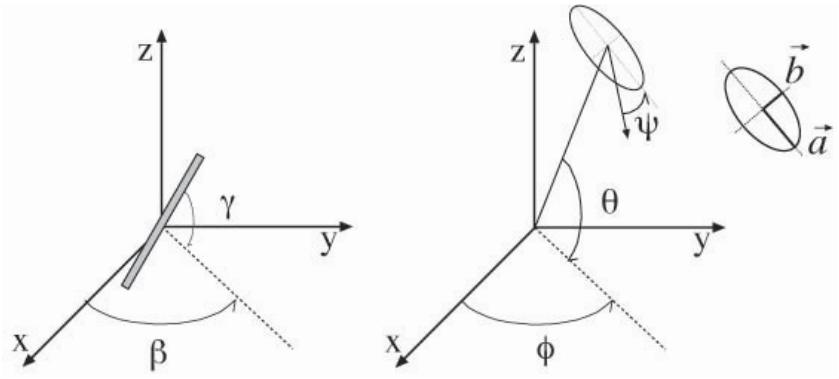

Figure 1.2: Illustration of the angles used for the numerical description of the sensor and the orientation of an ellipse in 3-D space.

4.2 Total Field and Power Flux Density Reconstruction

Computation of the power density in general requires knowledge of the electric (E-) and magnetic (H-) field amplitudes and phases in the plane of incidence. Reconstruction of these quantities from pseudo-vector E-field measurements is feasible, as they are constrained by Maxwell's equations. We have developed a reconstruction approach based on the Gerchberg-Saxton algorithm [2], [3], which benefits from the availability of the E-field polarization ellipse information obtained with the EUmmWV2 probe. This reconstruction algorithm, together with the ability of the probe to measure extremely close to the source without perturbing the field, permits reconstruction of the E- and H-fields, as well as of the power density, on measurement planes located as near as $\lambda/5$ away.

4.3 Power Flux Density Averaging

The average of the reconstructed power density is evaluated over a circular area in each measurement plane. The area of the circle is defined by the user; the default is 1 cm^2. The computed peak average value is displayed in the box at the top right. Note that the average is only evaluated for grid points where the averaging circle is completely filled with values; for points at the edge where the averaging circle is only partly filled with values, the averaged power density is set to zero.

4.4 Results Visualization

Once a measurement has been completed, the averaged power density and the averaging area used for calculation are displayed in the Project Overview window. Revaluation with a different averaging area is possible via the context menu.

The reconstructed E-field, H-field, and power-flux density can be visualized by clicking on the eye icon. The quantity to be displayed is selected in the Connection drop-down box of the Options window.

Three viewers are available:

- the slice viewer is used to visualize the E-field, H-field (both RMS), or power-density amplitude;
- the vector viewer is used to visualize the E-field, H-field, and power-density direction and amplitude at the same time. Note that it displays the magnitude of the E-field and H-field phasors, not RMS values;
- the grid viewer is not used in the currently released version.

A laptop device has been measured at 62 GHz (Figure 1.4.). The scan was performed in a plane at 5 mm from the antenna location. Figure 1.5a shows the measured E_{total}, while the reconstructed Poynting vector is shown in Figure 1.5b. The averaged S in 1 cm^2 is 3.94 W/m^2.

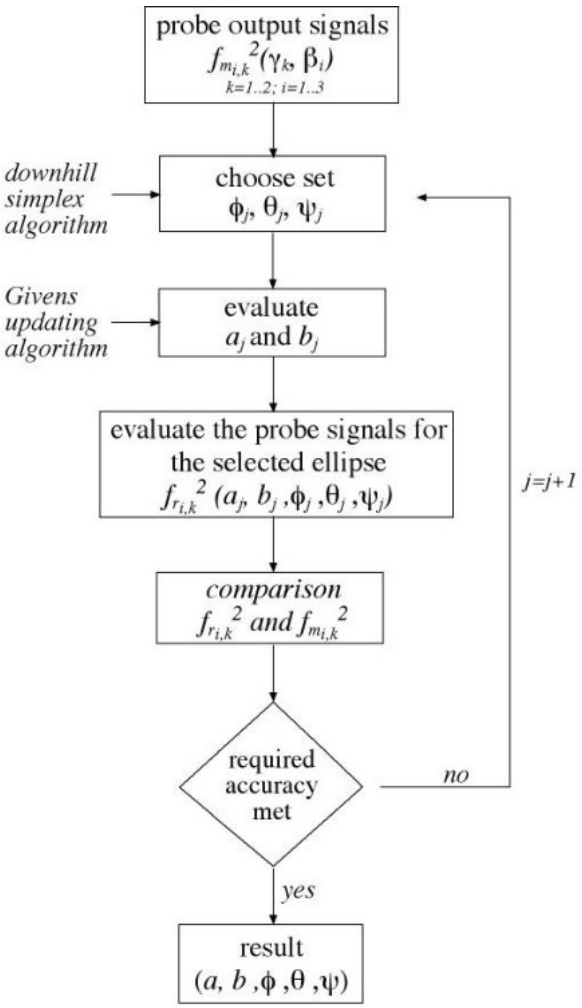

Figure 1.3: Numerical algorithm for reconstructing the ellipse parameters.

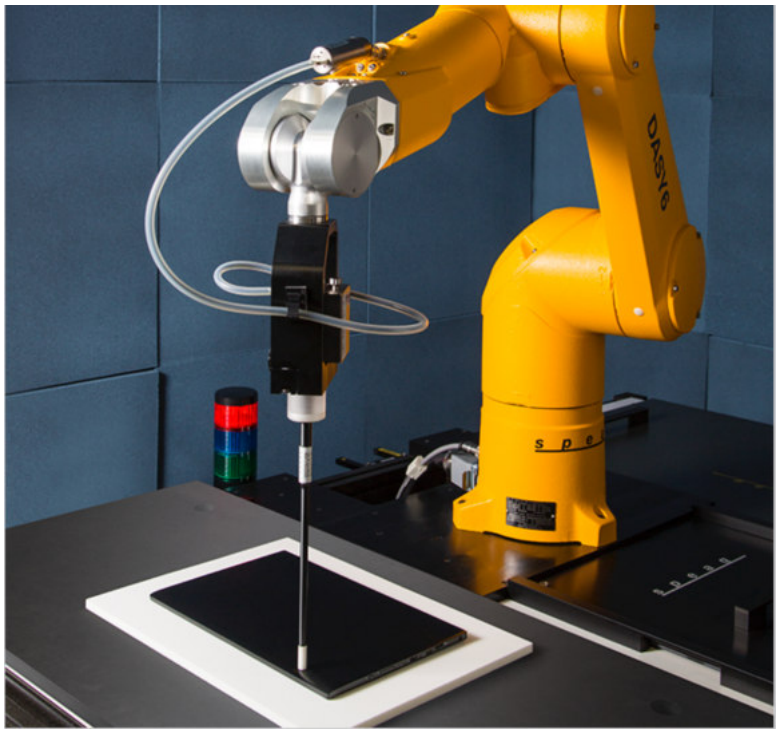

Figure 1.4: Laptop device during measuring with DASY6 system at 62 GHz.

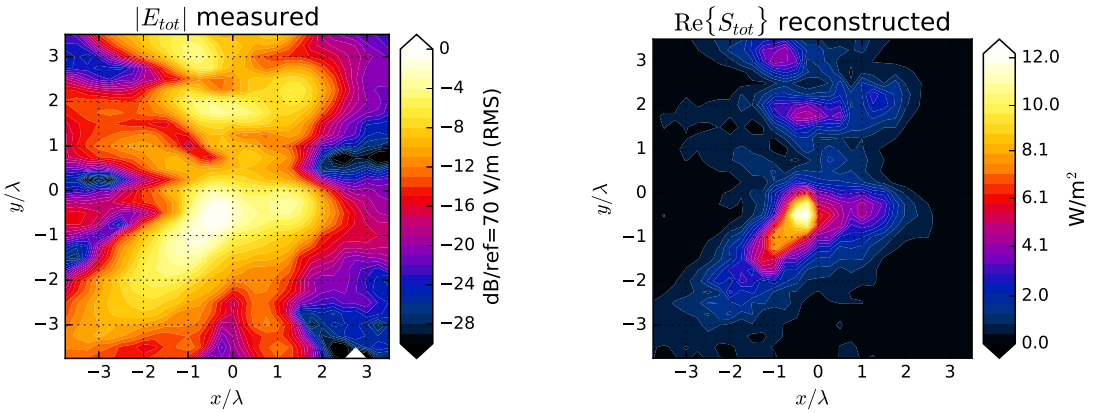

(a) Measured E-field at 5 mm from a laptop device at 62 GHz.

(b) Reconstructed Poynting vector at 5 mm from a laptop device at 62 GHz.

Figure 1.5: Example measurement result of a laptop at 62 GHz (see picture above).

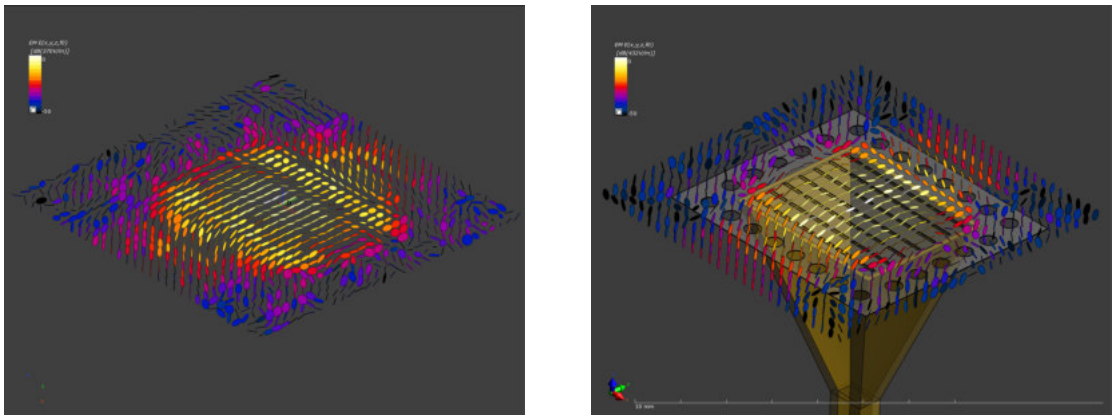

(a) Measured polarization ellipse.

(b) Simulated polarization ellipse.

Figure 1.6: Measured and Simulated polarization ellipse at 2 mm from the slotted array defined in Section 7 at 30 GHz.

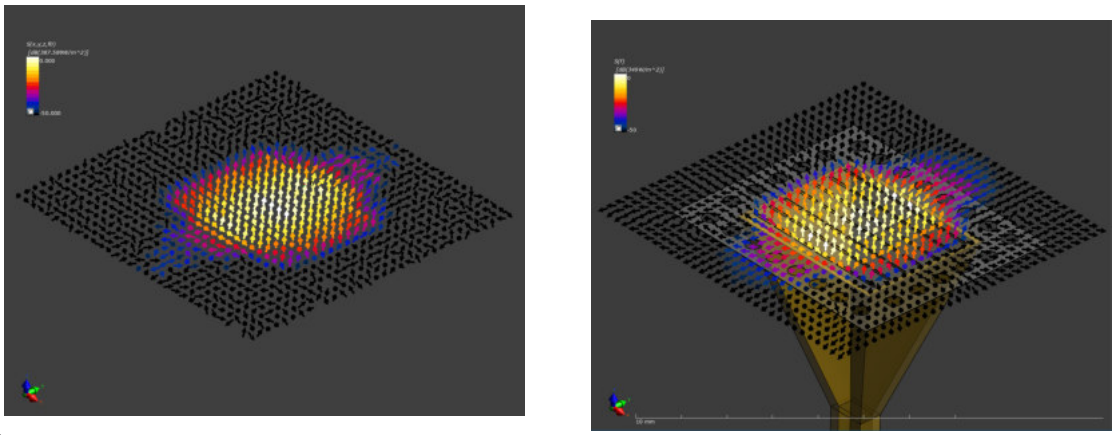

(a) Reconstructed Poynting vector from the E-field measurements.

(b) Simulated Poynting vector.

Figure 1.7: Measured and simulated Poynting vector at 2 mm from the slotted array defined in Section 7 at 30 GHz.

5 Reporting

5.1 Measurement Printout

Measurement printouts can be generated as described below:

- Go to Measurement mode.
- Click on a Measurement Group to be exported in Project Overview view. The Report tool is now enabled.
- Click on the Report tool and select the desired reporting format.
- Select the template file in the file selection dialog and click on Open.

A printout of the selected measurement group is now available. It is located in the same folder as the template file. Two export formats are currently supported, Word and HTML. The layout can be customized by the end user.

5.2 Summary Table

The summary table is a covenient tool to have an overview on the measurement results. The E-, H- fields as well as power density and averaged power density can be visualized for each measurements. The table can be exported to various formats. An example is shown on Figure 1.8

Phantom	Test Distance	Position	Description	Channel	Frequency	UID	Revision	Measurement Group Name	Job Name	Avg. Area [cm2]	Avg. Power Density [W/m2]	Peak Power Density [W/m2]	Peak E-field [V/m]	Peak H-field [A/m]
5G	2.5	FRONT (SCREEN)	CW	30000	30000.0 MHz	0	-	Measurement Group	5G Scan	1.0	516	865	538	1.61
5G	5.0	FRONT (SCREEN)	CW	30000	30000.0 MHz	0	-	Measurement Group	5G Scan	1.0	453	804	513	1.57
5G	10.0	FRONT (SCREEN)	CW	30000	30000.0 MHz	0	-	Measurement Group	5G Scan	1.0	388	495	416	1.21
5G	20.0	FRONT (SCREEN)	CW	30000	30000.0 MHz	0	-	Measurement Group	5G Scan	1.0	291	349	371	0.995

Figure 1.8: Example of Summary Table for Measurements at Different Distances.

6 Uncertainty

The uncertainty budget shown in Table 1.1 for *5G Module V1.0* has been adapted from the IEC62209 standard series and is consistent with the current draft of the IEC106 WG10 report. The budget, which is very preliminary and valid only for the frequency range from 28 – 90 GHz, reflects the state of knowledge and performance for probe calibration and the *5G Module V1.0* as of May 2017.

Preliminary *5G Module V1.0* Uncertainty Budget
Evaluation Distances to the Antennas ≤50 mm and the Freqeuncy Range 28 – 90 GHz
Based on the 62209 Standard Family

Error Description	Uncertainty Value (±dB)	Probability Distribution	Div.	(c_i)	Std. Unc. (±dB)	(v_i) v_{eff}
Measurement System						
Probe Calibration[c]	0.43	N	1	1	0.43	∞
Hemispherical Isotropy	0.60	R	$\sqrt{3}$	1	0.35	∞
Linearity	0.2	R	$\sqrt{3}$	1	0.12	∞
System Detection Limits	0.04	R	$\sqrt{3}$	1	0.02	∞
Modulation Response[m]	0.1	R	$\sqrt{3}$	1	0.06	∞
Readout Electronics	0.01	N	1	1	0.01	∞
Response Time	0.03	R	$\sqrt{3}$	1	0.02	∞
Integration Time	0.11	R	$\sqrt{3}$	1	0.06	∞
RF Ambient Noise	0.04	R	$\sqrt{3}$	1	0.02	∞
RF Ambient Reflections	0.21	R	$\sqrt{3}$	1	0.12	∞
Probe Positioner	0.04	R	$\sqrt{3}$	1	0.02	∞
Probe Positioning	0.11	R	$\sqrt{3}$	1	0.06	∞
S_{avg} Reconstruction[r]	0.61	R	$\sqrt{3}$	1	0.35	∞
Test Sample Related						
Power Drift	0.21	R	$\sqrt{3}$	1	0.12	∞
Power Scaling[p]	0.0	R	$\sqrt{3}$	1	0.0	∞
Combined Std. Uncertainty					0.7	∞
Expanded Std. Uncertainty					**1.4**	

Table 1.1: Preliminary uncertainty budget for *5G Module V1.0* based on the IEC 62209 standard family and in compliance with the WG10 draft report. The budget is valid for the frequency range 28 – 90 GHz and represents a worst-case analysis. For specific tests and configurations, the uncertainty could be considerably smaller.

Footnotes: [c] The probe is calibrated in the far-field over horn antennas. Each antenna is characterized for the E-field at the calibration distance. The field is determined by means of a three-antenna method with identical horns at different distances, evaluating the power over a fine frequency raster, thereby reducing ripple caused by mismatches and reflections in the setup. In addition, the resulting sensitivities available typically every 5 GHz are fit to a probe sensor model further averaging outliers at single frequencies and is valid for frequencies down to 700 MHz. The resulting frequency-dependent parameters (sensitivity and probe angles) are hence dominated by the power measurement, source-power drift, and spectral purity, and the probe isotropy deviation in the far field in combination with reflections. [m] SMC calibration is a new method for determining the total deviation from linearity. [r] Reconstruction uncertainty for a given E-field input that meets the scanning requirements, i.e., grid extension of 80 mm, steps of $< \lambda/4$, and plane separation of $\lambda/4$; [p] if power scaling is used.

7 Validation

The validation reported here is a subset of the validation requirements currently developed for the WG10 of IEC106.

7.1 Validation Antennas

The development of the emerging 5G technology for wireless devices requires free-space measurements of antenna arrays that operate at millimeter wave frequencies. Two validation antenna arrays consisting of electric dipoles and magnetic dipoles have been simulated and fabricated and have been measured at 30 GHz with the 5G module of cDASY6. A validation antenna array consisting of magnetic dipoles have been also simulated, fabricated and measured at 60 GHz.

7.1.1 Cavity-Fed Dipole Array at 30 GHz

This antenna consists of an array of nine dipoles arranged in an irregular lattice. The dipoles (0.8 mm × 1.86 mm) are excited by non-resonant slots (1.9 mm × 0.4 mm) sharing a 0.508 mm dielectric substrate with relative permittivity $\epsilon_r = 3.63$. The excitation modes are generated by a resonant cavity (21.18 mm × 21.18 mm × 5.0 mm), which is fed by an SMA connector situated underneath. This array has been optimized to function at 30 GHz with a reflection coefficient better than −25 dB. The fabricated prototype has been tuned with screws placed perpendicular to the dipoles. The dipole array is shown in Figs. 1.9a and 1.9b.

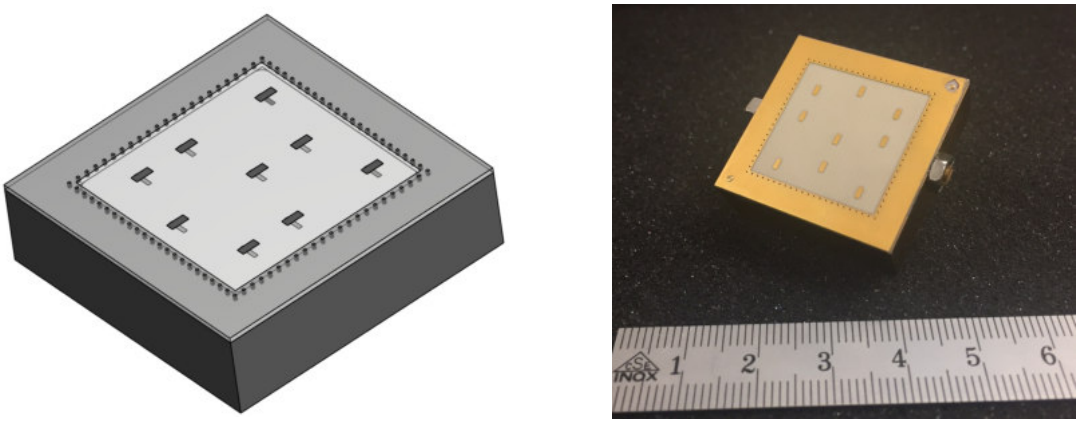

(a) Schematic diagram of the dipole array.

(b) Photo of the dipole array.

Figure 1.9: Dipole array AA9D30GV1 operating at 30 GHz

7.1.2 Pyramidal Horn Loaded with an Array of Slot Antennas at 30 GHz

This antenna consists of a pyramidal horn loaded with an array of slot antennas on the aperture. A 20 dBi commercial horn (SAR-2013-28-S2) manufactured by SAGE Millimeter, Inc. was used (http://www.sagemillimeter.com/), while the array of rectangular slots was fabricated in a 0.15 mm stainless steel sheet (63 mm × 54 mm) by means of a laser cut stencil process and fixed to the horn aperture with conductive glue. This validation antenna has been optimized to operate in the frequency band from 29 to 31 GHz with a reflection coefficient better than −20 dB. The array has 42 resonant elements (5.4 mm × 0.8 mm) arranged in a 6 × 7 grid. The antenna generates a broadside pencil-beam perpendicular to the array plane in the far-field. The schematic diagram of the horn loaded with the slot array and a photo of the fabricated prototype are shown in Figs. 1.10a and 1.10b, respectively.

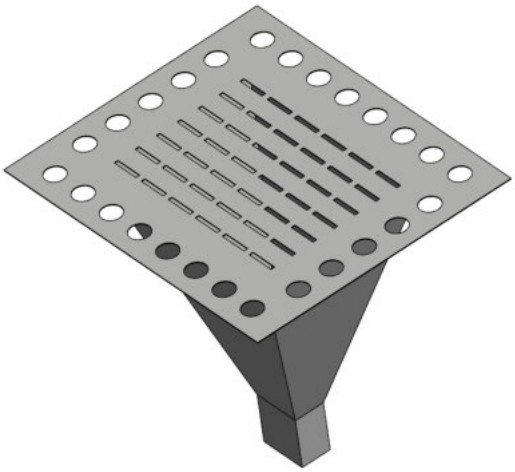

(a) Schematic of the pyramidal horn loaded with an array of slot antennas operating at 30 GHz.

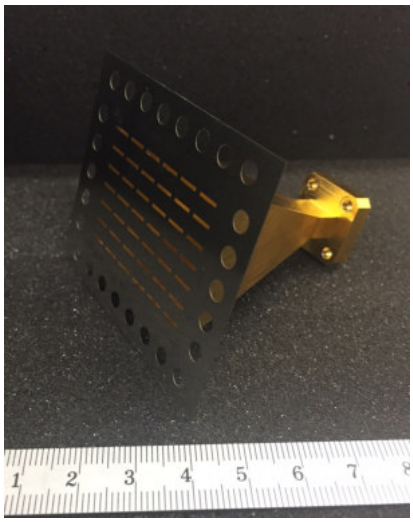

(b) Photo of the pyramidal horn loaded with an array of slot antennas.

Figure 1.10: Pyramidal horn loaded with an array of slot antennas (AA42S30GV1) operating at 30 GHz.

7.1.3 Pyramidal Horn Loaded with an Array of Slot Antennas at 60 GHz

This antenna consists of a pyramidal horn loaded with an array of slot antennas on the aperture. A 20 dBi commercial horn (SAR-2013-15-S2) manufactured by SAGE Millimeter, Inc. was used (http://www.sagemillimeter.com/), while the array of rectangular slots was fabricated in a 0.15 mm stainless steel sheet (23.4 mm × 18.8 mm) by means of a laser cut stencil process and fixed to the horn aperture with conductive glue. This validation antenna has been optimized to operate in the frequency band from 58 to 62 GHz with a reflection coefficient better than −15 dB. The array has 40 resonant elements (2.75 mm × 0.42 mm) arranged in a 5 × 8 grid. The antenna generates a broadside pencil-beam perpendicular to the array plane in the far-field. The schematic diagram of the horn loaded with the slot array and a photo of the fabricated prototype are shown in Figs. 1.11a and1.11b, respectively.

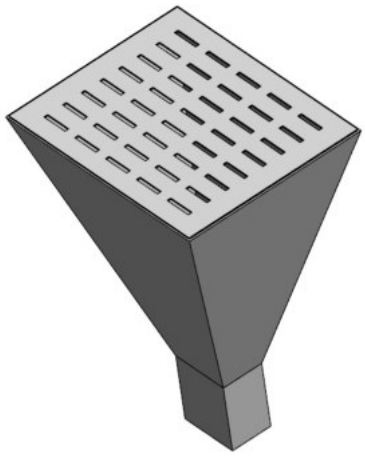

(a) Schematic of the pyramidal horn loaded with an array of slot antennas.

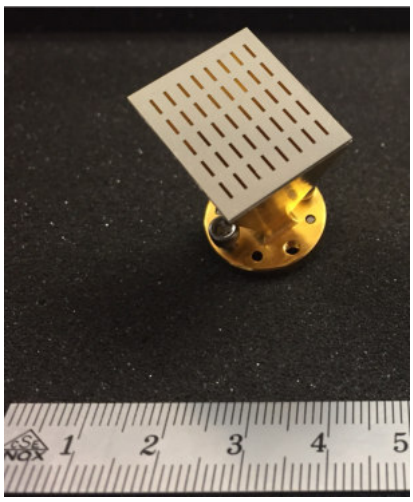

(b) Schematic of the pyramidal horn loaded with an array of slot antennas.

Figure 1.11: Pyramidal horn loaded with an array of slot antennas (AA40S60GV1) operating at 60 GHz.

7.2 Measurement Protocol

The validation horn has a waveguide flange interface and requires a waveguide source with calibrated input power at the flange interface. Because the EUmmW probe is wideband, the unwanted in- and out-band harmonics of the continuous wave signal at the calibration frequency must be well suppressed, typically by −20 dBc. The flange interface should be placed horizontally with the horn on top and the scan performed with the probe oriented vertically in the horn bore-sight axis. The scanning plane (sensor distance) is 10 mm above the flare surface of the horn. High resolution ($\leq \lambda/4$) settings must be used to determine the maxima of the pattern with sufficient precision (see Figure 1.12), and the result must be scaled to the calibrated power.

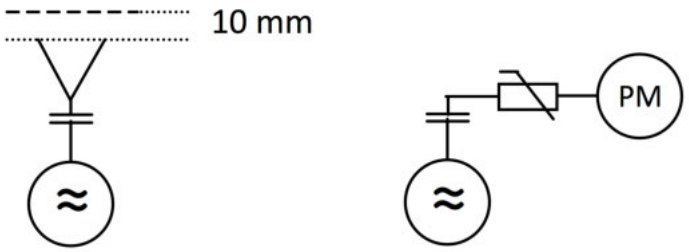

Figure 1.12: Sketch of the source setup for validation.

7.3 Results

The preliminary results of measurements performed at 10 GHz are summarized in Table 1.2, results at 30 GHz are summarized in Tables 1.3 and 1.4, results at 60 GHz are found in Tables 1.5 and results at 90 GHz are summarized in Table 1.6. The target values have been determined by simulations using SEMCAD X V16.2 (SPEAG, Switzerland) and the antenna input power normalized to the values at distance 50 mm.

The measured E_{total}, reconstructed H-field and reconstructed power density for the dipole array are shown in Figure 1.13, Figure 1.14 and Figure 1.15, respectively and compared to the simulation results at 30 GHz, 10 mm from the array surface.

	simulated		**measured**		**deviation**	
distance	E_{total}	$S_{avg1cm2}$	E_{total}	$S_{avg1cm2}$	E_{total}	$S_{avg1cm2}$
(mm)	(V/m)	(W/m^2)	(V/m)	(W/m^2)	(dB)	(dB)
2.00	490.08	201.87	437.12	166.27	-1.0	-0.7
5.00	253.88	112.22	234.29	96.74	-0.7	-0.6
10.00	164.11	75.88	166.78	72.15	0.1	-0.2
25.00	152.67	66.82	153.98	58.55	0.1	-0.6

Table 1.2: Comparison of the target values determined by simulation for the Pyramidal Horn loaded with Slot Array (AA18S10GV1 SN: 1001) normalized to the input power of 20 dBm at 10 GHz and compared to measurements made with the 5G Module V1.0 and the EUmmWV2 SN 9350 probe.

	simulated		measured		deviation	
distance	E_{total}	$S_{avg1cm2}$	E_{total}	$S_{avg1cm2}$	E_{total}	$S_{avg1cm2}$
(mm)	(V/m)	(W/m^2)	(V/m)	(W/m^2)	(dB)	(dB)
2.00	422.54	131.37	374.38	112.43	-1.1	-0.7
4.50	269.02	116.31	290.79	89.77	0.7	-1.1
10.00	303.64	119.83	278.91	101.38	-0.7	-0.7
12.50	302.29	121.05	263.08	94.20	-1.2	-1.1
50.00	121.32	36.31	121.32	33.60	0.0	-0.3

Table 1.3: Comparison of the target values determined by simulation for the Dipole Array (AA9D30GV1 SN: 1001) normalized to the input power of 20 dBm at 30 GHz and compared to measurements made with the 5G Module V1.0 and the EUmmWV2 SN 9350 probe.

	simulated		measured		deviation	
distance	E_{total}	$S_{avg1cm2}$	E_{total}	$S_{avg1cm2}$	E_{total}	$S_{avg1cm2}$
(mm)	(V/m)	(W/m^2)	(V/m)	(W/m^2)	(dB)	(dB)
2.00	357.74	169.09	378.05	224.42	0.5	1.2
4.50	302.78	152.37	345.26	191.26	1.1	1.0
10.00	256.61	138.35	272.63	165.97	0.5	0.8
12.50	262.68	133.31	274.54	148.65	0.4	0.5
50.00	182.32	80.97	182.32	80.07	0.0	-0.1

Table 1.4: Comparison of the target values determined by simulation for the Pyramidal Horn loaded with Slot Array (AA42S30GV1 SN: 1001) normalized to the input power of 20 dBm at 30 GHz and compared to measurements made with the 5G Module V1.0 and the EUmmWV2 SN 9350 probe.

	simulated		measured		deviation	
distance	E_{total}	$S_{avg1cm2}$	E_{total}	$S_{avg1cm2}$	E_{total}	$S_{avg1cm2}$
(mm)	(V/m)	(W/m^2)	(V/m)	(W/m^2)	(dB)	(dB)
2.00	196.70	54.46	210.44	49.43	0.6	-0.4
3.25	177.11	50.34	203.61	43.41	1.2	-0.6
10.00	154.85	39.28	159.97	36.27	0.3	-0.4
11.25	145.43	37.55	152.3	34.62	0.4	-0.4
50.00	88.74	18.23	88.73	17.12	0.0	-0.3

Table 1.5: Comparison of the target values determined by simulation for the Pyramidal Horn loaded with slot array (AA40S60GV1 SN: 1001) at 60 GHz normalized to the input power of 10 dBm and compared to measurements with the 5G Module V1.0 and the EUmmWV2 SN 9350 probe.

	simulated		measured		deviation	
distance	E_{total}	$S_{avg1cm2}$	E_{total}	$S_{avg1cm2}$	E_{total}	$S_{avg1cm2}$
(mm)	(V/m)	(W/m^2)	(V/m)	(W/m^2)	(dB)	(dB)
2.00	192.72	45.5	161.79	35.79	-1.5	-1.0
2.83	179.57	43.78	171.37	39.21	-0.4	-0.5
5.00	167.92	39.28	164.56	34.81	-0.2	-0.5
5.83	161.32	37.85	166.12	33.36	0.3	-0.6
10.00	118.79	29.58	123.3	27.19	0.3	-0.4
10.83	118.78	28.29	112.71	25.23	-0.5	-0.5

Table 1.6: Comparison of the target values determined by simulation for the Pyramidal Horn loaded with Slot Array (AA48S90GV1 SN: 1001) normalized to the input power of 20 dBm at 90 GHz and compared to measurements made with the 5G Module V1.0 and the EUmmWV2 SN 9350 probe.

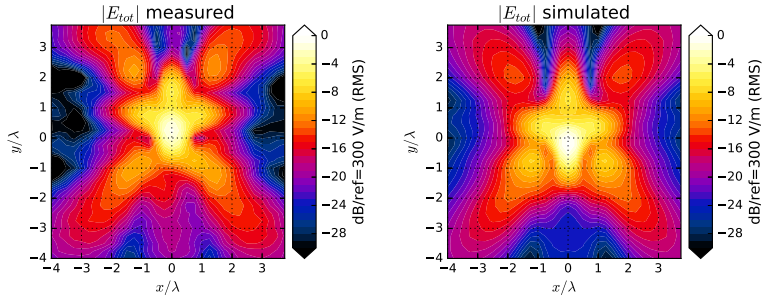

Figure 1.13: Measured E_{tot}-field compared to the results of the simulation of the dipole array validation system at 30 GHz.

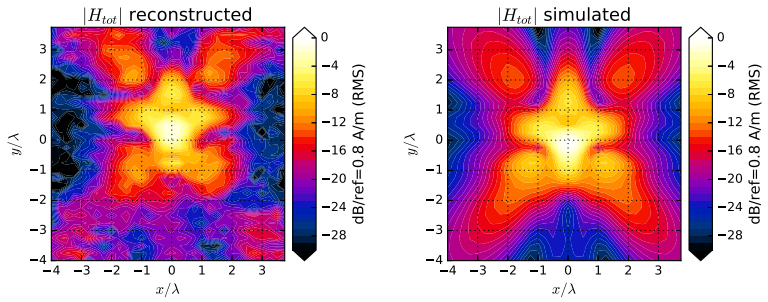

Figure 1.14: Reconstructed H-field of the measured data compared to the simulation results of the dipole array validation system at 30 GHz.

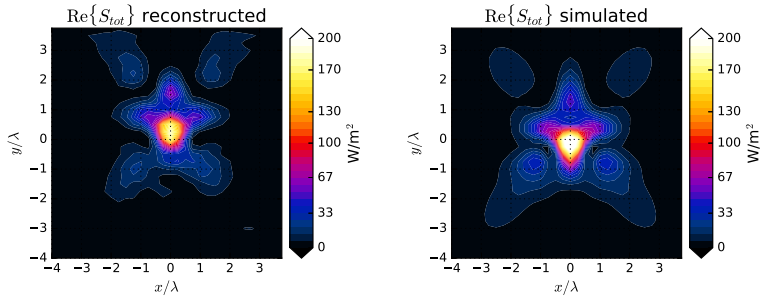

Figure 1.15: Reconstructed power-density field of the measured data compared to the simulation results of the dipole array validation system at 30 GHz.

8 Conclusions

This application note provides insight about the usage and performance of the 5G Module Version 1.0 of the 5G Module. Future versions of the 5G Module will empower evaluations of 5G transmitters with improved precision and with significantly reduced measurement time. The 5G Module will support evaluations on conformal surfaces in V2.0.

Bibliography

[1] K. Pokovic, T. Schmid, J. Frohlich, and N. Kuster. Novel probes and evaluation procedures to assess field magnitude and polarization. IEEE Transactions on Electromagnetic Compatibility 42(2): 240 – 244, 2000

[2] R. W. Gerchberg and W. O. Saxton. A practical algorithm for the determination of phase from image and diffraction plane pictures. Optik 35(2): 237 –ï£¡ï£¡ 246, 1972

[3] A. P. Anderson and S. Sali. New possibilities for phaseless microwave diagnostics. Part 1: Error reduction techniques. IEE Proceedings H - Microwaves, Antennas and Propagation 132(5): 291 –ï£¡ï£¡ 298, 1985